Soft Matter

PAPER

View Article Online
View Journal | View Issue

Cite this: *Soft Matter*, 2026, **22**, 2389

Liquid crystalline derivatives exhibiting smectic phases with ferro- and antiferro-electric properties

Natalia Podoliak, *[a] Vladimíra Novotná, [a] Terézia Jurkovičová, [a] Věra Hamplová, [a] Damian Pociecha [b] and Martin Cigl [a]

Received 12th January 2026,
Accepted 19th February 2026

DOI: 10.1039/d6sm00028b

rsc.li/soft-matter-journal

Chiral liquid crystalline molecules can self-assemble and generate ferroelectricity (FE) or antiferroelectricity (AF) in tilted lamellar smectic C phases. In previous studies, lactic acid has been repeatedly employed as an effective source of chirality. In this study, we synthesized several mesogens with the aim to establish the role of chiral chains and reveal their influence on the mesogenic and polar properties. For the first studied mesogen, we utilized a methylbutyl group in the chiral chain. The second mesogen differed from the first one in incorporated (*S*)-lactate group added to prolong the chain terminated with a methylbutyl. In the third homologue, two (*S*)-lactates and one methylbutyl group form the chiral chain. To establish their optical purity by high-performance liquid chromatography (HPLC), additional derivatives were prepared with a racemic methylbutyl chain. We compared all the homologues with respect to the effect of the chiral chain modification. Among them, the third derivative with two lactates in its chiral chain exhibited an AF smectic phase, which was stable and enantiotropic in a broad temperature range, including the room temperature, which could be attractive for various applications.

1. Introduction

Liquid crystals (LCs), as self-assemblies of organic molecules, belong to partially ordered soft matter systems. They can form various mesophases with specific properties. The introduction of chirality into the molecular structure of LCs can induce effects such as helicity or ferroelectricity.[1,2] Since the discovery of ferroelectricity in the tilted smectic C phase (SmC*) of chiral rod-like molecules, researchers have concentrated on investigating their electro-optical properties,[3–9] which are highly desirable for various applications due to their fast response and high contrast ratio. The antiferroelectric SmC_A* phase differs from the SmC* phase in the anticlinic ordering of the tilt angle in neighbouring layers and it shows greater relevance and potential in modern technological applications. Chiral liquid crystalline compounds have been intensively studied and analysed for various aspects of their molecular structure and the relationship between their molecular chirality and mesomorphic behaviour.[10]

Chirality can be introduced into molecular structures *via* a chiral part, and various chiral centres can be utilized for achieving this.[11–13] A lactate group is a promising source of chirality and its numerous derivatives have been synthesized to date.[14–20] In the previous design of lactate derivatives, (*S*)-lactate has been repeatedly utilized as a natural source of chirality. It has been demonstrated that these derivatives are thermally and chemically stable.[17–29] This type of chiral chains can enhance the chirality of liquid crystalline systems, which can be proved by the presence of various frustrated mesophases such as twist-grain boundary phases (TGB), smectic Q phase or blue phases.[25–27] The cholesteric phase, a chiral version of the nematic phase, with an unusually short pitch in the range of 120–250 nm, was described.[21] The pitch was detected by AFM analysis and confirmed by a resonant X-ray technique.[28] In several cases, it was found that the combination of two (*S*)-lactates in the chiral chain led to the presence of an antiferroelectric phase.[23–26]

For the estimation of the role of the molecular core, several series with (*S*)-lactate in the chiral chain have been investigated. Molecular cores with phenyls and biphenyls connected *via* ester linkages in various modifications and lateral substitutions have been prepared and studied.[17–20] The preference of smectic phases and the formation of ferroelectricity in SmC* has been described; nevertheless, very often there is a delicate balance between the SmC and orthogonal smectic A (SmA) phases, and a re-entrant SmA phase below the SmC phase has also been described.[29,30] In the previous study, we tried to establish how this effect can be influenced by chirality and prepared enantiomers with both (*S*)-lactate and (*R*)-lactate

[a] *Institute of Physics of the Czech Academy of Sciences, Na Slovance 1999/2, 18200, Prague, Czech Republic. E-mail: podoliak@fzu.cz*
[b] *Chemistry Department, Warsaw University, ul. Zwirki i Wigury 101, Warsaw, Poland*

groups. A detailed study confirmed that the mesomorphic properties do not vary when comparing enantiomers or their racemic mixtures and the re-entrant phenomenon is not connected with the chirality of the molecules.[30]

Herein, we concentrate on a molecular core based on phenyl–biphenyl connected *via* an ester linkage. This molecular structure was successfully applied previously and broadening of the mesophase range down to room temperature was achieved.[31] We investigated the effect of the chain length on the mesomorphic properties, and for this type of molecular core, we found that adding one more lactate into the chiral chain can induce antiferroelectricity.[23] Based on the same type of molecular core, we modified the chiral chain and varied it, starting from a simple methylbutyl and adding one or two (*S*)-lactate units. The chemical formulae of the studied compounds are presented in Fig. 1.

We synthesised three chiral compounds, namely, **Z12(*S*)**, containing an (*S*)-methylbutyl group; **ZL12(*S*,*S*)**, containing an (*S*)-lactate group and (*S*)-methylbutyl group, and **ZLL12(*S*,*S*,*S*)**, containing two (*S*)-lactate groups and an (*S*)-methylbutyl group. In addition, we prepared three analogous materials, in which methylbutyl was used in its racemic form: **Z12(*rac*)**, **ZL12(*S*,*rac*)** and **ZLL12(*S*,*S*,*rac*)**. These materials allowed us to identify the HPLC peaks corresponding to the opposite methylbutyl-containing (*R*) enantiomer, which is present in the **Z12(*rac*)**, **ZL12(*S*,*rac*)** and **ZLL12(*S*,*S*,*rac*)** compounds. Molecules of **Z12(*R*)**, **ZL12(*S*,*R*)** and **ZLL12(*S*,*S*,*R*)** could have been present in small amounts as impurities in the target substances **Z12(*S*)**, **ZL12(*S*,*S*)** and **ZLL12(*S*,*S*,*S*)**. Enantioselective HPLC methods were developed, and the separation conditions were optimized for each studied molecule. A detailed analysis and comparison allowed us to establish the optical purity of all the studied compounds.

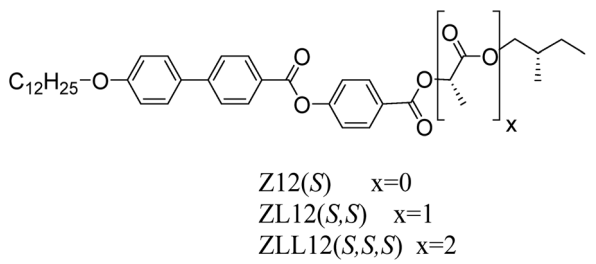

Fig. 1 Chemical formulae of the studied compounds: **Z12(*S*)**, **ZL12(*S*,*S*)** and **ZLL12(*S*,*S*,*S*)**.

2. Experimental

2.1. Synthesis of the Z12, ZL12 and ZLL12 materials

New liquid crystalline materials with multiple chiral centres were synthesised as shown in Scheme 1. The synthesis of the materials with one lactate unit **ZL12(*S*,*S*)** was analogous to that described previously.[31] Both types of materials, **ZL12(*S*,*S*)** and **ZL12(*S*,*rac*)**, were prepared in one step from 4′-(dodecyloxy)biphenyl-4-carboxylic acid (**1**), according to the general procedure described previously,[32] using an *N*,*N*′-dicyclohexylcarbodiimide (DCC)-mediated esterification reaction with chiral hydroxybenzoates **2** or **3**. Multichiral hydroxybenzoates **2** and **3** were synthesised in their pure enantiomeric forms as described earlier,[33] and their diastereomeric forms were synthesised in an analogous way. The detailed synthetic procedures are given in the SI.

2.2. Optical purity analysis

The optical purity of the materials was analysed using a high-performance liquid chromatography (HPLC) system on two chiral columns. The separation behaviour of **Z12(*S*)** was described and published previously.[34,35] For the materials with two and three chiral centres, **ZL12(*S*,*rac*)** and **ZLL12(*S*,*S*,*rac*)**, we developed new procedures for their analysis by enantioselective HPLC. For **ZL12(*S*,*rac*)**, we applied a chiral Lux i-Amylose-3 column (i.d. 4.6. and length 150 mm) from Phenomenex (USA) with amylose tris(3-chloro-5-methylphenylcarbamate) as a chiral selector. For the **ZLL12(*S*,*S*,*rac*)** material, we utilized a Lux Amylose-2 column (i.d. 4.6. and length 150 mm) from Phenomenex (USA) with amylose tris(5-chloro-2-methylphenylcarbamate) as a chiral selector. After enantiomer separation of the racemic materials, (*R*)-enantiomers were unambiguously identified only as a very small amount in the corresponding (*S*)-materials. Thus, all the compounds were confirmed to be optically highly pure, with purity higher than 98.2%, as shown in Table S1 in the SI.

2.3. Set-up and measurements

A polarized light optical microscope (POM), Nikon Eclipse E-600 (Nikon, Tokyo, Japan), equipped with a heating stage,

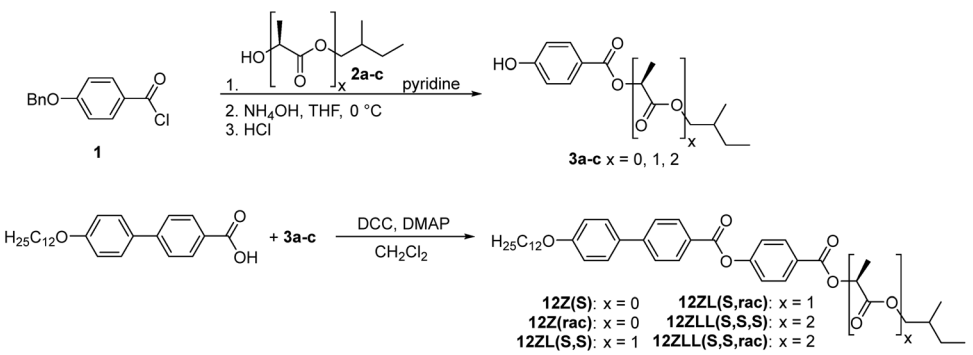

Scheme 1 Synthesis routes of the target materials.

Linkam LTSE350 (Linkam, Tadworth, UK), and a digital camera, Canon EOS 700D, were applied for textural observations and all electro-optical measurements. The temperature was changed at a rate of about 5 K min^{-1} and stabilized for texture acquisition with an accuracy ±0.1 K. We mostly studied our compounds in commercial cells (WAT, Warsaw, Poland), with glasses covered by transparent indium tin oxide (ITO) electrodes and surfactant coating to ensure a homogeneous geometry (HG). We filled the cells in the isotropic phase by means of capillary action.

We studied thermal properties by means of differential scanning calorimetry (DSC), utilizing a Pyris Diamond 7 calorimeter (PerkinElmer, Shelton, CT, USA). 1–3 mg of compounds were weighed and hermetically sealed in aluminium pans. The heating and cooling runs were conducted at 10 K min^{-1}. Analysis of the calorimetric results supplies information on the phase transition temperature, T_{tr}, and the corresponding enthalpy value, ΔH.

The spontaneous polarisation, P_S, and the tilt angle, θ, were studied under an applied electric field. The θ values were calculated from the angular difference between the extinction positions under the opposite sign of the applied DC electric field of about ±10 V μm^{-1}. The P_S values were obtained by integration of the polarisation current detected under the applied electric field of a triangular profile (with the magnitude of 10–20 V μm^{-1}) at a frequency of 10 Hz.

For dielectric spectroscopy, we utilized a Schlumberger 1260 impedance analyser and measured the frequency dispersion of the complex permittivity, ε^*, in the frequency range of 1 Hz–1 MHz. The temperature was stabilized within ±0.1 K during the frequency sweeps. We analysed the measured data using the Cole–Cole equation, as follows:

$$\varepsilon^* - \varepsilon_\infty = \frac{\Delta\varepsilon}{1 + (if/f_r)^{(1-\alpha)}} - i\left(\frac{\sigma}{2\pi\varepsilon_0 f^n} + Af^m\right) \quad (1)$$

Formula (1) contains additional terms corresponding to the low frequency contribution from conductivity, σ, and the high frequency contribution due to the resistance of the ITO electrodes, respectively. The parameter α lies between 0 and 1 and describes the distribution of relaxation, ε_0 is the permittivity of vacuum, ε_∞ the high frequency permittivity, and n, m, and A are other supporting fitting parameters. We fitted the real, ε', and imaginary, ε'', parts of the complex permittivity $\varepsilon^*(f) = \varepsilon' - i\varepsilon''$ simultaneously to formula (1) to obtain information on the relaxation frequency, f_r, and the dielectric strength, $\Delta\varepsilon$.

The small-angle X-ray scattering (SAXS) technique was applied to determine the structural properties of the studied compounds. The Bruker D8 Discover (Bruker AXS, Karlsruhe, Germany) was used, equipped with ceramic X-ray tube as a radiation source (Cu anode, wavelength λ = 1.5418 Å), parabolic mirror monochromator and scintillation counter. An Anton Paar DCS 350 chamber (Anton Paar, Graz, Austria) was used for temperature control with an accuracy of ±0.1 K. The samples were prepared in the form of thin films, and the measurements were performed in the reflection mode. The smectic layer thickness, d, was calculated using Bragg's law from the position of the diffraction angle peak.

3. Results

3.1. DSC measurements and texture observations

Differential scanning calorimetry (DSC) measurements allowed us to establish the phase transition temperatures and the corresponding enthalpies. The results obtained from the second run of DSC measurements are collected in Table 1. The DSC thermographs are shown in Fig. 2 for illustration. Firstly, the mesophases were identified based on the observations under a polarizing microscope. We concluded that all the studied compounds show two smectic mesophases. During the POM studies in planar (HG) cells, we observed fan-shaped and broken fan-shaped textures in the SmA and SmC phases, respectively. For illustration, the fan-shaped textures observed for the **ZL12(*S*,*S*)** compound in the SmA and SmC* phases are presented in Fig. 3. The textures for several other compounds could be found in the SI (Fig. S1–S4). In the SmC* phase, we detected a defect pattern (Fig. 3(b)), which can be ascribed to dechiralization lines, which exist in the SmC* phase due to anchoring at the cell surfaces.[36] However, the dechiralization lines were not regular, which prevented the measurement of the helical pitch of the SmC* phase. Nevertheless, we assume that the helical pitch is small because after the application of an electric field, dechiralization lines started appearing within the texture, depicting the helical structure unwinding (see Fig. S2 for **ZLL12(*S*,*S*,*rac*)**). For the compounds with two lactates, **ZLL12(*S*,*S*,*S*)** and **ZLL12(*S*,*S*,*rac*)**, there is a direct phase transition from the Iso to the SmC* phase on cooling. An additional tilted phase appeared during the cooling process, which is

Table 1 DSC data for the **Z12**, **ZL12** and **ZLL12** compounds, taken during the 2nd heating and cooling runs at a rate of 10 K min^{-1}. The melting point (m.p.), phase transition temperature (T_{tr}), temperature of crystallization (T_{cr}), and temperature of the isotropic–mesophase phase transition (T_{iso}) are presented in °C, and the corresponding enthalpy values (ΔH) are presented in kJ mol^{-1} in square brackets. M1 and M2 are the subsequent mesophases obtained upon cooling

Compounds	m.p. [ΔH]	T_{cr} [ΔH]	M2	T_{tr} [ΔH]	M1	T_{iso} [ΔH]
Z12(*S*)	75 [+18.16]	32 [−8.79]	SmC*	133 [−0.40]	SmA	175 [−3.58]
Z12(*rac*)	67 [+22.72]	30 [−19.62]	SmC	132 [−0.10]	SmA	175 [−5.81]
ZL12(*S*,*S*)	52 [+18.96]	35 [−17.86]	SmC*	115 [−0.33]	SmA	127 [−2.24]
ZL12(*S*,*rac*)	49 [+19.56]	38 [−16.68]	SmC*	114 [−0.25]	SmA	129 [−2.86]
ZLL12(*S*,*S*,*S*)	54 [+15.84]	35 [−12.26]	SmC_A*	91 [−0.06]	SmC*	98 [−0.88]
ZLL12(*S*,*S*,*rac*)	60 [+24.30]	37 [−17.71]	SmC_A*	91 [−0.08]	SmC*	99 [−0.61]

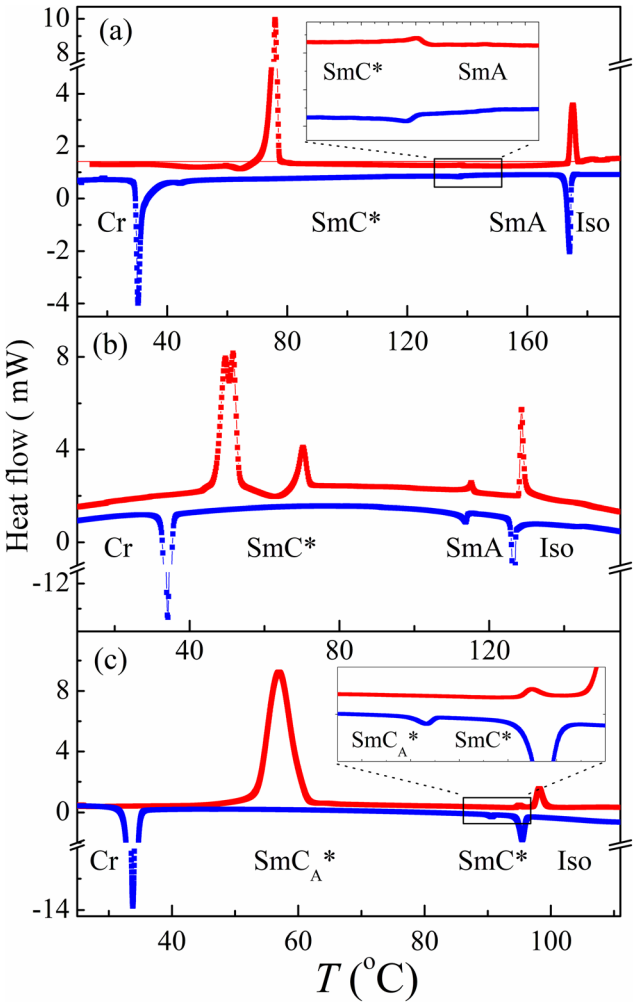

Fig. 2 DSC plots for the (a) **Z12(*S*)**, (b) **ZL12(*S*,*S*)** and (c) **ZLL12(*S*,*S*,*rac*)** compounds detected during the second heating (red) and cooling (blue) runs. Phase transitions with small enthalpy changes are presented in enlarged views in the insets.

recognized as a transformation between two broken fan-shaped textures (Fig. S3). It is interesting to note that for the racemic compound **Z12(*rac*)**, twisted domains were observed (Fig. S4), which evidences the separation of molecular conformers with different sense of axial chirality.[37]

3.2. Mesomorphic properties

For compound Z12 with a methylbutyl, we prepared and studied a chiral version, **Z12(*S*)**, and its racemic mixture, **Z12(*rac*)**. We observed that both compounds show an SmA–SmC phase sequence. In the case of **Z12(*S*)**, the SmC* phase reveals ferroelectricity, and we established its polar properties. We measured polarization, P_s, by integrating the switching current. The tilt angle, θ, was detected optically in an applied DC field. The temperature dependence of $P_s(T)$ and $\theta(T)$ is presented in Fig. 4 in comparison with other materials.

The compounds **ZL12(*S*,*S*)** and **ZL12(*S*,*rac*)** are both chiral and differ only in the terminal methylbutyl part. **ZL12(*S*,*rac*)** represents a molecular mixture of two chiral compounds,

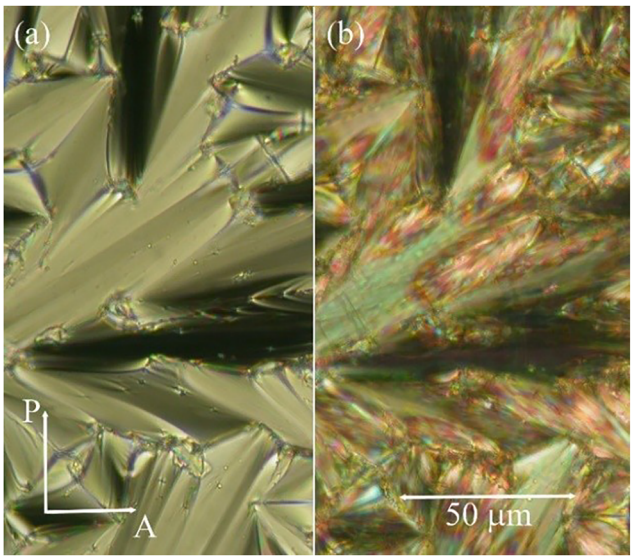

Fig. 3 Textures in the (a) SmA phase and (b) SmC* phase of **ZL12(*S*,*S*)** in a 7-μm planar cell.

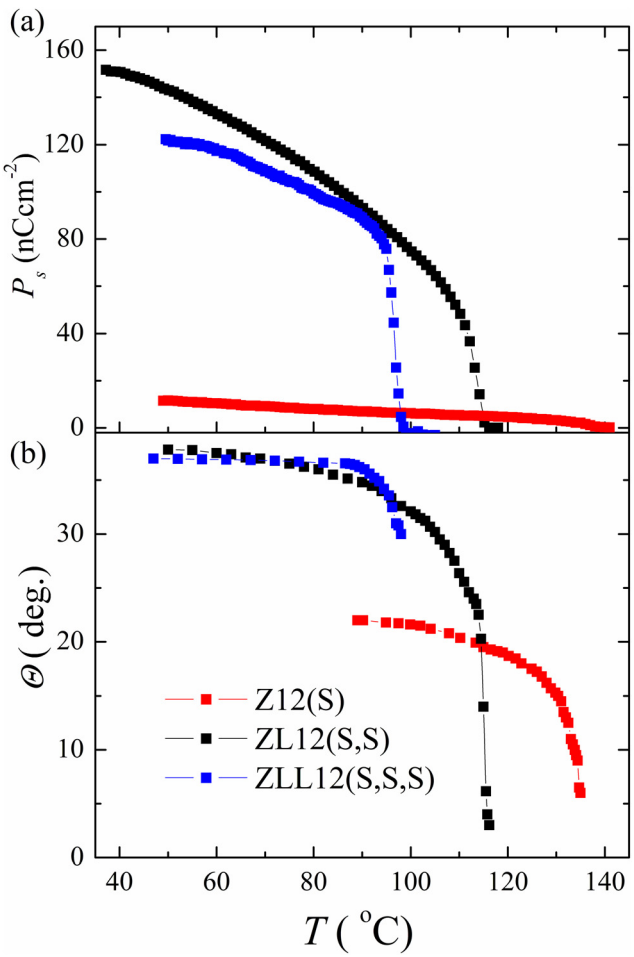

Fig. 4 Temperature dependence plots of the (a) spontaneous polarisation, P_s, and (b) tilt angle, θ, for the **Z12(*S*)**, **ZL12(*S*,*S*)** and **ZLL12(*S*,*S*,*S*)** compounds.

ZL12(*S*,*S*) and **ZL12(*S*,*R*)**, both of which we were able to distinguish by HPLC and establish their optical purity (for details, see SI). The mesomorphic properties of both compounds, **ZL12(*S*,*S*)** and **ZL12(*S*,*rac*)**, are similar, where the same SmA–SmC* phase sequence was detected on cooling from the isotropic phase. The comparison of the physical properties will be shown below.

The results for the two-lactate derivatives **ZLL12(*S*,*S*,*S*)** and **ZLL12(*S*,*S*,*rac*)** evidence that adding an additional lactate substantially decreases the phase transition temperature to the isotropic phase, T_{iso}. While compounds **Z12(*S*)**, **ZL12(*S*,*S*)** and **ZL12(*S*,*rac*)** exhibit the SmA–SmC* phase sequence and paraelectric-ferroelectric phase transition, for **ZLL12(*S*,*S*,*S*)** and **ZLL12(*S*,*S*,*rac*)**, we detected a direct phase transition from the isotropic phase to the SmC* phase at T = 98–99 °C on cooling. Then a transformation to the antiferroelectric SmC*$_A$ phase took place at the temperature T = 91 °C.

3.3. Polarization and tilt angle measurements

In the ferro- and antiferro-electric smectic mesophases, we measured the polarization and the tilt. The temperature dependence of these parameters is shown in Fig. 4 for **Z12(*S*)**, **ZL12(*S*,*S*)** and **ZLL12(*S*,*S*,*S*)**. One can see that the polarization values are much lower for the **Z12(*S*)** compound in comparison with the other two materials containing additional lactate groups. The polarization values of the racemic compounds **ZL12(*S*,*rac*)** and **ZLL12(*S*,*S*,*rac*)** do not differ much from their chiral counterparts **ZL12(*S*,*S*)** and **ZLL12(*S*,*S*,*S*)**, respectively. Explicitly, the P_s values for **Z12(*S*)** do not exceed 12 nC cm^{-2}, and for **ZL12(*S*,*S*)** and **ZL12(*S*,*rac*)** these values moderately saturate at about 120 nC cm^{-2}. For **ZLL12(*S*,*S*,*S*)** and **ZLL12(*S*,*S*,*rac*)**, their P_s values continuously increase and reach 160 nC cm^{-2} when approaching their crystallization temperature. Similarly, the tilt angle of **Z12(*S*)** does not extend 20°, while for the lactate derivatives **ZL12(*S*,*S*)** and **ZLL12(*S*,*S*,*S*)**, the value of θ approaches 40°. It is necessary to point out that for **ZLL12(*S*,*S*,*S*)** and **ZLL12(*S*,*S*,*rac*)**, no peculiarities are observed at the SmC*–SmC$_A$* phase transition in their $P_s(T)$ and $\theta(T)$ dependence. This can be explained by the high measuring applied electric field (20 V μm^{-1}) exceeding the threshold, which is necessary to unwind the helical structure and transform the sample from the anticlinic to synclinic state.[38] Moreover, this phase transition is not recognizable in the current profile during the polarization measurements. We were able to measure the non-zero polarization and tilt angle values at temperatures slightly exceeding the phase transition temperatures to the SmC* phase (Table 1) due to the electroclinic effect.

A more complicated situation is if we compare the polarization and the tilt values between **ZL12(*S*,*S*)** and **ZL12(*S*,*rac*)**. As was mentioned above, the polarization values do not show measurable differences between **ZL12(*S*,*S*)** and **ZL12(*S*,*rac*)**. On the contrary, we detected smaller tilt values for the racemic **Z12(*rac*)** in comparison with **Z12(*S*)**, and for **ZL12(*S*,*rac*)** in comparison with **ZL12(*S*,*S*)**, which is demonstrated in Fig. 5. Alternatively, for the longest derivatives **ZLL12(*S*,*S*,*S*)** and **ZLL12(*S*,*S*,*rac*)**, their tilt values jump up to 30° at the Iso-SmC* phase transition, and within the SmC* and SmC$_A$* phases, the tilt values increase up to 35° continuously on cooling of the sample, without a recognizable difference between these two derivatives. We can claim that the molecular shape of the ZLL12 derivatives with very long and complicated chiral chains is complex and the racemization at the terminal part only partially influences their molecular packing.

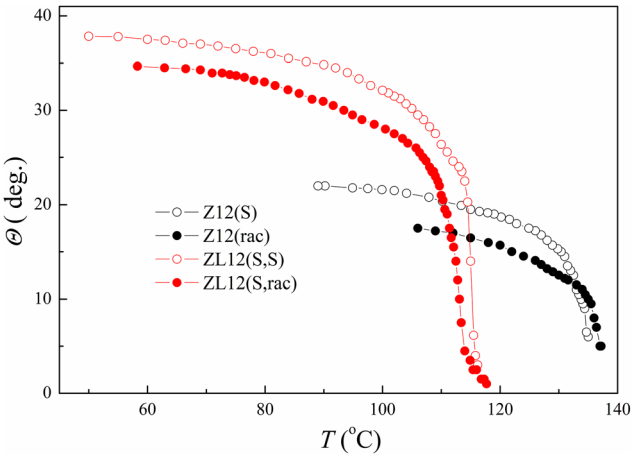

Fig. 5 Temperature dependence plot of the tilt angle, θ, for the **Z12(*S*)**, **Z12(*rac*)**, **ZL12(*S*,*S*)** and **ZL12(*S*,*rac*)** compounds.

3.4. Dielectric spectroscopy

Dielectric spectroscopy is a powerful tool to describe molecular dynamics, mainly in the vicinity of the paraelectric-ferroelectric SmA–SmC* phase transition. Due to molecular fluctuations, various modes can be observed with different characteristic behaviours.[39] A soft mode is detectable in the SmA phase, with a steep linear decrease in the relaxation frequency during cooling when approaching the SmA–SmC* phase transition. A phason type of mode, which is a Goldstone mode, can be detected in a ferroelectric phase, reflecting the vibrations of tilted molecules. For an antiferroelectric phase, the dynamics is even more complex in tilted smectics due to the opposite orientation of the tilted molecules in the neighbouring layers, and other modes can be detected.[40,41]

We performed dielectric spectroscopy measurements for all the studied derivatives. For **Z12(*rac*)**, which does not reveal a ferroelectric phase, its dielectric signals do not show any dispersion (see Fig. S5). For all the ferroelectric compounds, we detected one dielectric mode in their frequency scans. By fitting the complex permittivity, ε^*, to eqn (1), we obtained the temperature dependence of the dielectric strength, $\Delta\varepsilon(T)$, and the relaxation frequency, $f_r(T)$. For **Z12(*S*)**, the soft mode is observed at the SmA–SmC* transition, the Goldstone mode in the SmC* phase is rather weak and the value of the dielectric strength, $\Delta\varepsilon$, does not exceed 10 (see Fig. S6 in SI). For the lactate derivatives **ZL12(*S*,*S*)** and **ZL12(*S*,*rac*)**, in the SmC* phase, the Goldstone mode is much stronger in comparison with **Z12(*S*)**. The dielectric strength $\Delta\varepsilon(T)$ reaches a value of about 160 for **ZL12(*S*,*S*)**. Fig. 6 presents the temperature dependence of the fitted values of the dielectric strength, $\Delta\varepsilon$, and the

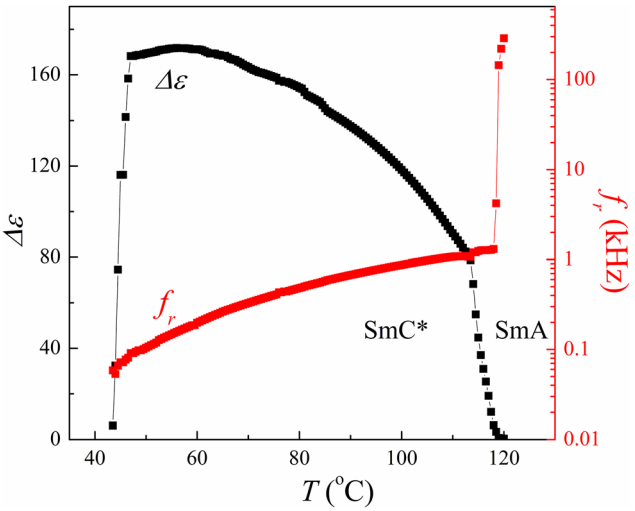

Fig. 6 Temperature dependence plot of the fitted values of the dielectric strength, $\Delta\varepsilon$, and the relaxation frequency, f_r, for **ZL12(*S*,*S*)**, measured in a 5-μm cell without a surfactant.

relaxation frequency, f_r, for **ZL12(*S*,*S*)**. When we compared the fitting results for **ZL12(*S*,*S*)** and **ZL12(*S*,*rac*)**, there are only small differences.

For **ZLL12(*S*,*S*,*S*)** with the SmC*–SmC$_A$* phase sequence, the Goldstone mode in SmC* is very strong and the $\Delta\varepsilon(T)$ values are very high, more than 300. Unfortunately, for frequencies higher than 100 kHz, there is a limitation in studying high-frequency modes due to the conductivity of ITO electrodes. Accordingly, to extend the frequency range of the dielectric measurements and achieve better accuracy, we utilized cells with more conductive gold electrodes. The measurements in cells with gold electrodes allowed us to extend the frequency range of the dielectric spectroscopy up to 10 MHz. For **ZLL12(*S*,*S*,*S*)** in a 7-μm gold cell, the 3D plots of the real, ε', and imaginary, ε'', parts of permittivity *versus* temperature and frequency are shown in Fig. 7(a) and (b), respectively. Due to the presence of a Goldstone mode, the permittivity values are very high in the SmC* phase and decrease at the SmC*–SmC$_A$* phase transition. In the SmC$_A$* phase, two very week modes are present. We fitted these modes and the results are presented in Fig. 8(a) and (b) for the dielectric strength, $\Delta\varepsilon$, and the relaxation frequency, f_r, respectively. This dielectric spectroscopy behaviour is characteristic for the antiferroelectric ordering of the observed smectic mesophase.[41]

3.5. X-ray diffraction measurements

The phase identification was confirmed by XRD measurements. In the X-ray profile, there are commensurate peaks reflecting the lamellar character of the smectic phases. According to the peak maximum position, we can obtain information about the layer spacing value, d. Fig. 9 shows the temperature dependence of $d(T)$ for **Z12(*S*)**, **ZL12(*S*,*S*)** and **ZLL12(*S*,*S*,*S*)**, with the corresponding intensity of their X-ray peak. For compounds **Z12(*S*)** and **ZL12(*S*,*S*)**, the $d(T)$ values continuously increase within the SmA phase during the cooling process, as shown in see Fig. 9(a) and (b), respectively. A negative thermal

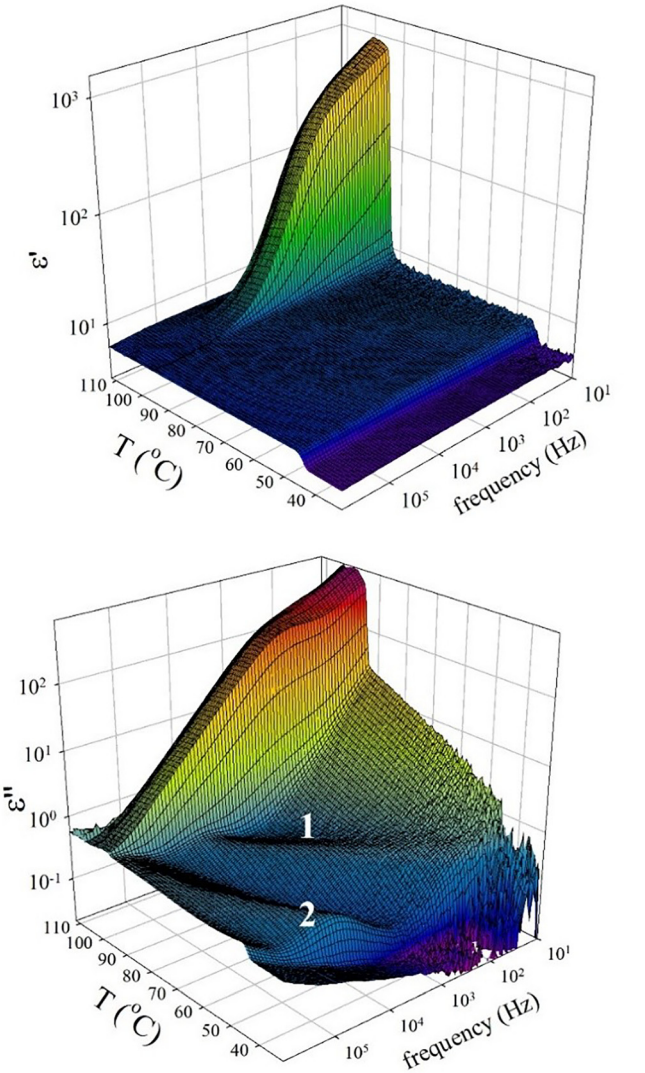

Fig. 7 (a) Real part of the complex permittivity, ε', and (b) imaginary part of the permittivity, ε'', in the SmC* and SmC$_A$* phases of **ZLL12(*S*,*S*,*S*)**. Dielectric spectroscopy was performed in a 7-μm cell with gold electrodes. Numbers mark the two modes in the SmC$_A$* phase, namely, 1: a lower-frequency mode and 2: a higher-frequency mode.

expansion coefficient is typical for the SmA phase for rod-like molecules, which can be explained by stretching of their terminal chains and growth of orientational order of molecules upon cooling. When entering the tilted SmC* phase from the SmA phase, the layer spacing decreased gradually, which reflects the tilting of the molecules in layers. During the cooling of the sample within the SmC* phase, the decrease in $d(T)$ became slower and finally the layer spacing was slightly increasing till the crystallization temperature. This effect can be explained by the continuous stretching of the terminal molecular chains and extension of the molecules. This increase in molecular length compensates for the changes in layer thickness due to the tilt, which tends to a gradual saturation (Fig. 4 and 5).

For the ZLL12 compounds with the SmC* phase forming directly below the isotropic phase, the layer spacing decreases

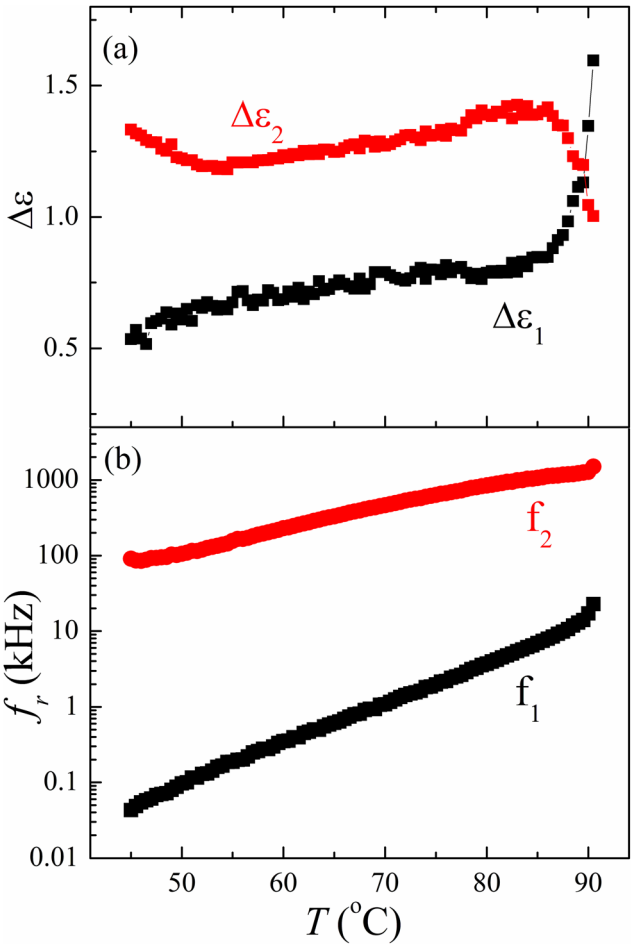

Fig. 8 Fitted values of (a) dielectric strength, $\Delta\varepsilon$, and (b) relaxation frequency, f_r, for the two modes detected in the SmC_A^* phase, where the red colour indicates the higher-frequency mode and the black colour indicates the lower-frequency mode.

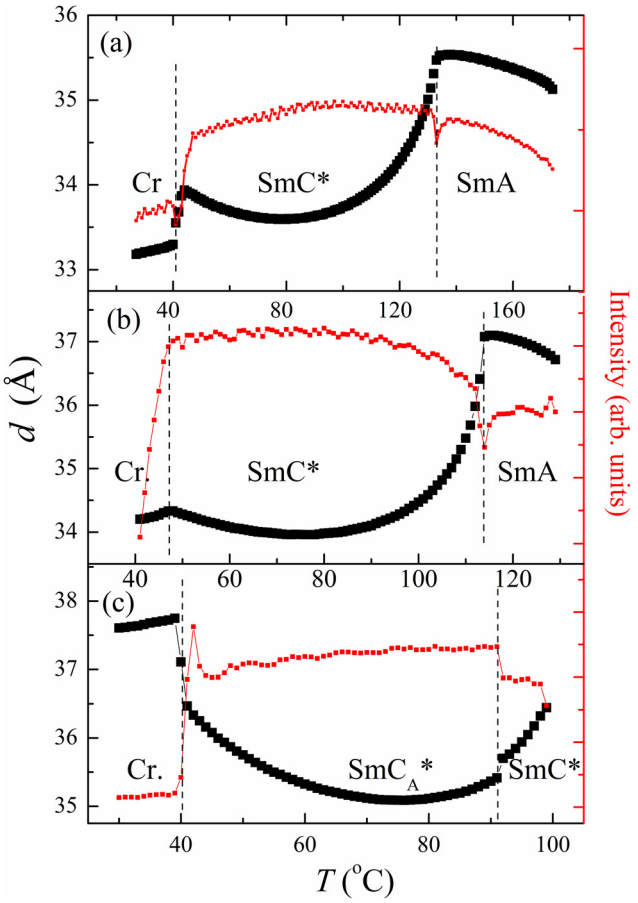

Fig. 9 Temperature dependence plots of the layer spacing, d, and the corresponding intensity of the X-ray diffraction signal for (a) **Z12(*S*)**, (b) **ZL12(*S*,*S*)** and (c) **ZLL12(*S*,*S*,*S*)**.

within the SmC* phase until the phase transition to SmC_A^*, where $d(T)$ slightly jumps down, as shown in Fig. 9(c) for **ZLL12(*S*,*S*,*S*)**. This small decrease is usually attributed to the better molecular ordering in the anticlinic phase. Simultaneously, an increase in diffracted intensity is observed (Fig. 9(c)), which is usually explained by an increase in smectic order due to the enhanced packing efficiency of the anticlinic arrangement.[26,33,42] The profile of $d(T)$ continuously changes within the SmC_A^* phase, but it is not monotonous. Below the SmC*–SmC_A^* phase transition, the layer spacing continues decreasing, and after reaching a local minimum, starts growing deeper in the SmC_A^* phase. Concerning the effect of racemization on the layer spacing values, there is a negligible change when comparing **ZL12(*S*,*S*)** with **ZL12(*S*,*rac*)** or **ZLL12(*S*,*S*,*S*)** with **ZLL12(*S*,*S*,*rac*)**.

We can linearly extrapolate the layer spacing from the SmA phase and calculate the tilt angle from the temperature dependence, $d(T)$, in the SmC* phase, θ_X. The tilt obtained from the layer spacing is usually lower than that determined from the orientation of the optical axis under a microscope. The reason for this is that the optical axis relates to the orientation of the molecular core, while the layer spacing reflects the overall molecular shape. As the terminal chains are very long, they can be inclined from the molecular core, which results in a smaller calculated molecular tilt.[18] Fig. S8 in the SI presents the temperature dependence of the tilt angle measured optically, θ, and the tilt calculated from the temperature dependence of the layer spacing measured by SAXS, θ_X, for **Z12(*S*)** and **ZL12(*S*,*S*)**.

3.6. DFT and *ab initio* calculations

To obtain detailed information about the studied molecules, we optimized their molecular structures using *ab initio* calculations at the B3LYP 6-31Gd level of theory.[43] The resulting molecules in their global minimum potential energy conformation are shown in Fig. 10. We established the length of the molecule, l, with extended terminal chains to be about 37.4 Å for **Z12(*S*)** and **Z12(*rac*)**. For **ZL12(*S*,*S*)** and **ZL12(*S*,*rac*)**, their l values were calculated to be about 39.6 Å. These values are slightly higher than the values of the layer spacing in the SmA phase, which evidences that in the mesophase, molecular shape does not correspond to the fully extended conformation. For **ZLL12(*S*,*S*,*S*)** and **ZLL12(*S*,*S*,*rac*)**, with the most conformationally complicated chiral chain, we evaluated their molecular length to be $l \sim 39.2$ Å. Nevertheless, we cannot compare l with

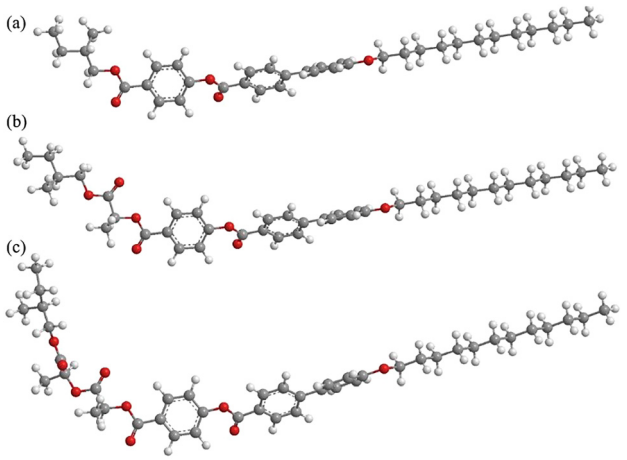

Fig. 10 Visualization of the molecular structures of the studied molecules of (a) **Z12(*S*)**, (b) **ZL12(*S*,*S*)** and (c) **ZLL12(*S*,*S*,*S*)** generated using the Chem3D program.

the layer spacing, as there are only tilted SmC phases present in the phase sequence. We can speculate that the large bend in the chiral terminal chain obtained by DFT optimisation will be lower in the condensed fluid state within the smectic layers as the molecules experience lateral collisions.

4. Discussion and conclusions

Chiral rod-like molecules represent a vivid and attractive topic in liquid crystals from many aspects, spanning basic research to applications. In this contribution, we aimed to shed more light on the effect of the chiral chain and its partial racemization in the methylbutyl terminal part. We prepared and studied chiral mesogens with an equivalent molecular core and modified only their chiral chain. We applied a methylbutyl chain, *S*-lactate methylbutyl and two lactates with a methylbutyl in the chiral chain, respectively, in three molecular structures. Additionally, we prepared analogous compounds with racemic methylbutyl to prove the effect of the racemization at this position.

Firstly, we compared the mesomorphic properties with respect to the molecular length and shape. We found a large reduction in the phase transition temperature, T_{iso}, with the molecular elongation. This effect has been observed previously for various compounds. For multilactate derivatives, it has been established that adding one more lactate to a molecular structure can drop the temperatures by even more than 30 °C.[17,23] Alternatively, for all the studied compounds herein, the crystallization temperatures and melting points are similar, which means that the width of the liquid crystalline phases decreases with the incorporation of an additional lactate group into the chain. We observed an antiferroelectric phase (SmC_A^*) only for the compounds with two lactates with a methylbutyl in the chiral chain. We identified this phase based on the decrease in permittivity at the SmC*–SmC_A^* transition and the emergence of two weak modes. The anticlinicity of the SmC_A^* phase was supported by POM observations, in which only a sufficiently high electric field causes the helices to unwind and switching to be detected. In addition, the slight jump-like decrease in the temperature dependence of the layer spacing $d(T)$ at the SmC*–SmC_A^* phase transition and the simultaneous increase in the diffracted intensity, which are probably connected with an increase in the smectic order, support the synclinic-anticlinic transformation.

We applied DFT calculations to shed more light on the molecular structure. When comparing the molecular shape and the overall length, we must consider the tendency of molecular chains to crimp. For the shortest molecules **Z12(*S*)** and **Z12(*rac*)**, the layer spacing approximately corresponds to the molecular length, l, of their most extended conformation. However, this is not true for the longer molecules **ZL12(*S*,*S*)** and **ZL12(*S*,*rac*)**, for which their layer spacing is smaller than their l value. For compounds **ZLL12(*S*,*S*,*S*)** and **ZLL12(*S*,*S*,*rac*)**, we cannot compare the data, as there is no orthogonal SmA phase in the phase sequence.

We tried to compare the polarization values of the three basic molecular structures. Unambiguously, it turned out that **Z12(*S*)** shows much lower P_s values than lactic acid derivatives ZL12 and ZLL12. This necessarily leads to the conclusion that (*S*)-lactate is actually very effective in supporting strong ferroelectric behaviour. When comparing **ZL12(*S*,*S*)** with **ZL12(*S*,*rac*)** and **ZLL12(*S*,*S*,*S*)** with **ZLL(*S*,*S*,*rac*)**, one can see that their polarization values are similar and the effect of racemization in the methylbutyl part is not pronounced enough. We can conclude that the replacement of *S*-methylbutyl with methylbutyl racemate does not play an important role in polarization and dielectric properties.

Conversely, the tilt values for **Z12(*rac*)** and **ZL12(*S*,*rac*)** show slightly smaller values than their counterparts **Z12(*S*)** and **ZL12(*S*,*S*)**, respectively. This fact can be explained by the lower degree of ordering in the presence of various enantiomeric versions, which imply a greater diversity of molecular conformations, which necessarily leads to worse packing. We can conclude that racemization at methylbutyl only slightly influenced the ferroelectric properties of the lactate derivatives and lactate seems to be a driving force to enhance their ferroelectric properties.

Author contributions

NP – Data curation, formal analysis, investigation, validation, visualisation, and writing – original draft, review and editing; VN – conceptualisation, data curation, funding acquisition, project administration, supervision, visualisation, and writing – original draft, review and editing; TJ – formal analysis, investigation, validation, and writing – original draft; VH – conceptualization, methodology, project administration, and supervision; DP – formal analysis, investigation, validation, visualisation, and writing – original draft; and MC – formal analysis, resources, validation, and writing – original draft.

Conflicts of interest

No potential conflict of interest was reported by the authors.

Data availability

The data supporting this article have been included as part of the supplementary information (SI). Supplementary information: includes the synthesis procedures, NMR spectra, chemical and optical purity (Table S1), and further experimental details. See DOI: https://doi.org/10.1039/d6sm00028b.

Acknowledgements

This work was supported by the Czech Ministry of Education, Youth and Sports through the international project 8I23001 FerroFluid (EIG Concert Japan – 9th Call, ''Design of Materials with Atomic Precision'').

References

1 I. Dierking, Chiral Liquid Crystals: Structures, Phases, Effects, *Symmetry*, 2014, **6**, 444–472, DOI: 10.3390/sym6020444.
2 H.-S. Kitzerow and C. Bahn, *Chirality in Liquid Crystals*, Springer-Verlag, New York, 2001.
3 D. M. Walba, S. C. Slater, W. N. Thurmes, N. A. Clark, M. A. Handschy and F. Supon, Design and synthesis of a new ferroelectric liquid crystal family. Liquid crystals containing a nonracemic 2-alkoxy-1-propoxy unit, *J. Am. Chem. Soc.*, 1986, **108**(17), 5210–5221.
4 M. Tykarska and A. Drzewicz, Effect of molecular structure and temperature on the helical pitch and handedness in Antiferroelectric liquid crystalline phase, *J. Mol. Liq.*, 2019, **292**, 110379, DOI: 10.1016/j.molliq.2019.01.148.
5 M. Zurowska, M. Filipowicz, M. Czerwinski and M. Szala, Synthesis and properties of ferro- and antiferroelectric esters with a chiral centre based on (S)-(+)-3-octanol, *Liq. Cryst.*, 2019, **46**, 299–308, DOI: 10.1080/02678292.2018.1499147.
6 J. Herman and P. Kula, The synthesis of chiral fluorinated 4-alkyl-4′-[(4-alkylphenyl)ethynyl]biphenyls, *Tetrahedron Lett.*, 2013, **54**, 3621–3623, DOI: 10.1016/j.tetlet.2013.04.118.
7 D. Gupta, P. Kula and A. Bhattacharjee, Mesomorphic, electro-optic and dielectric behaviour of a semi-fluorinated chiral liquid crystalline material forming polar smectic phases, *J. Mol. Struct.*, 2020, **1219**, 128557, DOI: 10.1016/j.molstruc.2020.128557.
8 M. Zurowska, J. Dziaduszek, M. Szala, P. Morawiak and A. Bubnov, Effect of lateral fluorine substitution far from the chiral center on mesomorphic behaviour of highly titled antiferroelectric (S) and (R) enantiomers, *J. Mol. Liq.*, 2018, **267**, 504–510, DOI: 10.1016/j.molliq.2017.12.114.
9 K. Milewska, W. Drzewiński, M. Czerwiński and R. Dąbrowski, Design, synthesis and mesomorphic properties of chiral benzoates and fluorobenzoates with direct SmC_A^*-Iso phase transition, *Liq. Cryst.*, 2015, **42**, 1601–1611, DOI: 10.1080/02678292.2015.1078916.
10 C. Tschierske, Development of Structural Complexity by Liquid-Crystal Self-assembly, *Angew. Chem., Int. Ed.*, 2013, **52**, 8828–8878, DOI: 10.1002/anie.201300872.
11 J. Fitas, A. Dłubacz, P. Fryn, M. Marzec, T. Jaworska-Golab, A. Deptuch, K. Kurp, M. Tykarska and M. Zurowska, New •ferroelectric and antiferroelectric liquid crystals studied by complementary methods, *Liq. Cryst.*, 2016, **44**, 566–576, DOI: 10.1080/02678292.2016.1225841.
12 M. Zurowska, R. Dabrowski, J. Dziaduszek, K. Garbat, M. Filipowicz, M. Tykarska, W. Rejmer, K. Czuprynski, A. Spadlo, N. Bennis and J. M. Otón, Influence of alkoxy chain length and fluorosubstitution on mesogenic and spectral properties of high tilted antiferroelectric esters, *J. Mater. Chem.*, 2011, **21**, 2144–2153, DOI: 10.1039/C0JM02015J.
13 A. Deptuch, S. Lalik, M. Jasiurkowska-Delaporte, E. Juszyńska-Gałązka, A. Drzewicz, M. Urbańska and M. Marzec, Comparative study of electrooptic, dielectric, and structural properties of two glassforming antiferroelectric mixtures with a high tilt angle, *Phys. Rev. E*, 2022, **105**, 024705, DOI: 10.1103/PhysRevE.105.024705.
14 F. Brombach, J. M. Neudoerfl and D. Blunk, The chiral pool as valuable natural source: new chiral mesogens made from lactic acid, *Mol. Cryst. Liq. Cryst.*, 2011, **542**, 62–74, DOI: 10.1080/15421406.2011.569689.
15 W.-L. Tsai and H. L. Kuo, Ferroelectric liquid crystals containing a 2(S)-[2(S)-methylbutoxy]propionyloxy unit, *Liq. Cryst.*, 1993, **13**, 765–773, DOI: 10.1080/02678299308027292.
16 S. L. Wu and F.-S. Lai, Synthesis and ferroelectric properties of new chiral liquid crystals derived from (S)-lactic acid with alkoxyethanols, *Liq. Cryst.*, 2005, **32**, 1243–1249, DOI: 10.1080/02678290500139799.
17 V. Hamplová, V. Novotná and M. Kašpar, Lactic acid derivatives with three-phenyl ring molecular core: Design and mesomorphic properties, *Ferroelectrics*, 2014, **468**, 18–27, DOI: 10.1080/00150193.2014.932655.
18 V. Novotná, V. Hamplová, M. Kašpar, N. Podoliak, A. Bubnov, M. Glogarová, D. Nonnenmacher and F. Giesselmann, The effect of lactate unit number in compounds with azo group in the molecular core, *Liq. Cryst.*, 2011, **38**, 649–655, DOI: 10.1080/02678292.2011.565426.
19 V. Hamplová, A. Bubnov, M. Kašpar, V. Novotná, D. Pociecha and M. Glogarová, New ferroelectric and antiferroelectric liquid crystalline materials containing different numbers of lactate units, *Liq. Cryst.*, 2003, **30**, 627–631, DOI: 10.1080/026782903100010695.
20 N. Podoliak, V. Novotná, M. Kašpar, V. Hamplová, M. Glogarová and D. Pociecha, Anomalous phase sequence in new chiral liquid crystalline materials, *Liq. Cryst.*, 2014, **41**, 176–183, DOI: 10.1080/02678292.2013.846424.
21 V. Novotná, V. Hamplová, M. Glogarová, L. Lejček and E. Gorecka, Effect of the applied electric field on new cholesterics with extremely short pitch, *Liq. Cryst.*, 2018, **45**, 634–640, DOI: 10.1080/02678292.2017.1376126.
22 M. Kašpar, V. Novotná, V. Hamplová and O. Pacherová, The effect of the alkyl chain length on the mesomorphic properties of new lactic acid derivatives, *Liq. Cryst.*, 2014, **41**, 1179–1187, DOI: 10.1080/02678292.2014.910315.
23 A. Bubnov, V. Novotná, V. Hamplová, M. Kašpar and M. Glogarová, Effect of multilactate chiral part of liquid

crystalline molecule on mesomorphic behaviour, *J. Mol. Struct.*, 2008, **892**, 151–157, DOI: 10.1016/j.molstruc.2008.05.016.

24 V. Novotná, V. Hamplová, M. Kašpar, N. Podoliak and D. Pociecha, Variety of mesophases in compounds with an increasing number of lactate units in the chiral chain, *Liq. Cryst.*, 2013, **40**, 14–21, DOI: 10.1080/02678292.2012.730638.

25 M. Kašpar, V. Novotná, V. Hamplová, D. Pociecha and M. Glogarová, Phase diagram of new lactic acid derivatives exhibiting ferro- and antiferroelectric phases, *Liq. Cryst.*, 2008, **35**, 975–985, DOI: 10.1080/02678290802308043.

26 V. Novotná, M. Kašpar, V. Hamplová, N. Podoliak, M. Glogarová and D. Pociecha, Ferroelectric, antiferroelectric and TGB phases in lactic acid derivatives, *Liq. Cryst.*, 2012, **39**, 477–486, DOI: 10.1080/02678292.2011.653411.

27 M. Kašpar, P. Bílková, A. Bubnov, V. Hamplová, V. Novotná, M. Glogarová, K. Knížek and D. Pociecha, New chlorine-substituted liquid crystals possessing frustrated TGBA and SmQ phases, *Liq. Cryst.*, 2008, **35**, 641–651, DOI: 10.1080/02678290802056212.

28 A. Smekhova, V. Novotná, L. Fekete, R. Abrudan, M. Fondell, V. Hamplová and B. Ostrovskii, Ultra-short helix pitch and spiral ordering in cholesteric liquid crystal revealed by resonant soft X-ray scattering, *Soft Matter*, 2022, **18**, 89–96, DOI: 10.1039/d1sm01543e.

29 V. Novotná, V. Hamplová, N. Podoliak, M. Kašpar, M. Glogarová, D. Pociecha and E. Gorecka, Chiral liquid crystalline compounds with a re-entrant SmA* phase, *J. Mater. Chem.*, 2011, **21**, 14807–14814, DOI: 10.1039/c1jm12131f.

30 V. Novotná, S. Stulov, M. Cigl, V. Hamplová, E. Gorecka and D. Pociecha, Mesomorphic properties of lactic acid derivatives and their racemic mixtures in comparison with analogous non-chiral compounds, *Liq. Cryst.*, 2020, (47), 1516–1527, DOI: 10.1080/02678292.2020.1741040.

31 N. Podoliak, V. Novotná, V. Hamplová, D. Pociecha and M. Cigl, Structural optimisation of lactic acid derivatives to obtain enhanced ferroelectric properties in smectic phases, *Liq. Cryst.*, 2023, **50**, 149–156, DOI: 10.1080/02678292.2022.2131917.

32 M. Kaspar, V. Hamplová, V. Novotná, M. Glogarová, D. Pociecha and P. Vanek, New series of ferroelectric liquid crystals with two or three chiral centres exhibiting antiferroelectric and hexatic phases, *Liq. Cryst.*, 2001, **28**, 1203–1209, DOI: 10.1080/02678290110051602.

33 N. Podoliak, M. Cigl, V. Hamplová, D. Pociecha and V. Novotná, Multichiral liquid crystals based on terphenyl core laterally substituted by chlorine atom, *J. Mol. Liq.*, 2021, **336**, 116267, DOI: 10.1016/j.molliq.2021.116267.

34 P. Vaňkátová, A. Kubíčková and K. Kalíková, How mobile phase composition and column temperature affect enantiomer elution order of liquid crystals on amylose tris(3-chloro-5-methylphenylcarbamate) as chiral selector, *Electrophoresis*, 2021, **42**, 1844–1852, DOI: 10.1002/elps.202000350.

35 P. Vaňkátová and A. Kubíčková, Towards greener enantioselective liquid chromatography: An exploratory study on chiral liquid crystals, *Anal. Chim. Acta*, 2025, **1342**, 343664, DOI: 10.1016/j.aca.2025.343664.

36 M. Glogarova and J. Pavel, The structure of chiral SmC* liquid crystals in planar samples and its change in an electric field, *J. Phys.*, 1984, **45**, 143–149, DOI: 10.1051/jphys:01984004501014300.

37 M. Glogarova, F. Hampl, L. Lejcek, V. Novotna, J. Svoboda and M. Cigl, Communication: Experimental proof of symmetry breaking in tilted smectics composed of molecules with axial chirality, *J. Chem. Phys.*, 2010, **133**, 221102, DOI: 10.1063/1.3525644.

38 S. T. Lagerwall, *Ferroelectric and Antiferroelectric Liquid Crystals*, Wiley-VCH, Weinheim, 1999.

39 L. A. Parry-Jones and S. J. Elston, Theoretical prediction of the dielectric spectrum of an antiferroelectric liquid crystal, *J. Appl. Phys.*, 2002, **92**, 449–455, DOI: 10.1063/1.1486029.

40 P. Perkowski, M. Mrukiewicz, M. Zurowska, R. Dabrowski and L. Jaroszewicz, Dielectric modes in antiferroelectric liquid crystal observed at low temperatures, *Liq. Cryst.*, 2013, **40**, 864–870, DOI: 10.1080/02678292.2013.795622.

41 P. Perkowski and M. Urbanska, Dielectric modes in antiferroelectric and ferroelectric liquid crystals in a pure enantiomeric version and a racemic mixture, *Materials*, 2024, **17**, 3335, DOI: 10.3390/ma17133335.

42 I. Muševič, R. Blinc and B. Žekš, *The Physics of Ferroelectric and Antiferroelectric Liquid Crystals*, World Scientific, Singapore, 2000.

43 A. A. Granovsky, Firefly version 8, https://classic.chem.msu.su/gran/firefly/index.html.

